



# Architecture Dependence on the Dynamics of Nano-LiFePO<sub>4</sub> Electrodes



Bernardo Orvananos<sup>a</sup>, Rahul Malik<sup>b</sup>, Hui-Chia Yu<sup>a</sup>, Aziz Abdellahi<sup>b</sup>, Clare P. Grey<sup>c,d</sup>, Gerbrand Ceder<sup>b</sup>, Katsuyo Thornton<sup>a,\*</sup>

<sup>a</sup> Department of Materials Science and Engineering, University of Michigan, Ann Arbor, MI 48109

<sup>b</sup> Department of Materials Science and Engineering, Massachusetts Institute of Technology, Cambridge, MA 02139

<sup>c</sup> Department of Chemistry, University of Cambridge, Cambridge, CB2 1EW, UK

<sup>d</sup> Department of Chemistry, Stony Brook University, Stony Brook, NY 11794

## ARTICLE INFO

### Article history:

Received 16 April 2014

Accepted 4 June 2014

Available online 12 June 2014

## ABSTRACT

Elucidating the role of interparticle Li transport and multi-particle (de)lithiation kinetics in nanoparticulate two-phase electrode materials such as LiFePO<sub>4</sub> is a challenging task because of the small temporal and spatial scale associated with the process. Often, the relevant processes that determine the kinetics of (dis)charging an electrode are assumed to be exclusively those associated with Li transport to and from the counter-electrode, without a consideration of interactions between particles. However, the redistribution of Li between nanoparticles can have a strong influence on the overall cell rate performance. Using a continuum model to simulate the lithiation kinetics of a porous aggregate of LiFePO<sub>4</sub> nanoparticles, we demonstrate the impact of cell architecture (in terms of ionic and electronic connectivities between active particles) and cycling rate on the multi-particle (de)lithiation kinetics. Specifically, the connectivity between particles is shown to have a strong effect on “interparticle phase separation,” a process by which active particles undergo additional cycling (charge during the overall discharge) and amplified reaction rates. We show that interparticle phase separation can be reduced or eliminated by improving (“homogenizing”) the connectivity between particles. Extensive comparisons to experimental literature and insights toward improving the performance of nanoparticulate electrodes are also provided.

© 2014 Elsevier Ltd. All rights reserved.

## 1. Introduction

To ensure long-term safety and reliability of Li-ion battery systems, special attention must be devoted to avoid overcharging/overdischarging the cathode since it can lead to accelerated degradation of the material and, at worst, thermal runaway. For large-scale Li-ion battery systems (e.g., in electric vehicles) to function successfully, these issues must be adequately addressed to avoid costly failures that currently impede widespread deployment of large battery systems [1]. Developing the solutions requires a detailed understanding of the relation between the battery's measurable properties (voltage, charge/discharge history, etc.) and the state of charge (SOC) of individual particles within the electrode. This can be especially challenging in nanoparticulate materials because their dynamics may differ from those of larger particles, and their study is complicated by their small size and

fast transformation. In a conventional porous electrode, many active particles ( $\sim 10^{10} - 10^{17}$ ) [2] are ionically (through the electrolyte) and electronically (through carbon-coating, carbon black, or particle-particle contact) linked to each other. Therefore, a particle network is formed in which Li can be transported not only between cathode and anode, but also between the active particles *within* the cathode.

If the cathode material remains as a single phase at equilibrium with respect to Li concentration for the relevant cycling range (as in LiTiS<sub>2</sub>, for instance [3]), then there is always a thermodynamic driving force to homogenize the Li concentration amongst all active particles. In these cases, a voltage reading across the cell also provides an accurate picture of each particle SOC. However, for phase-separating systems (where Li-poor and Li-rich phases are thermodynamically more stable than the uniform mixture), the interactions between particles are much more nuanced, and particles within the electrode can coexist in equilibrium at very different SOCs from one another and in many different configurations, all within a very narrow potential range [2,4]. In some materials, such as nanoparticulate lithium iron phosphate, LiFePO<sub>4</sub>,

\* Corresponding author. Tel.: +7346151498  
E-mail address: [kthorn@umich.edu](mailto:kthorn@umich.edu) (K. Thornton).

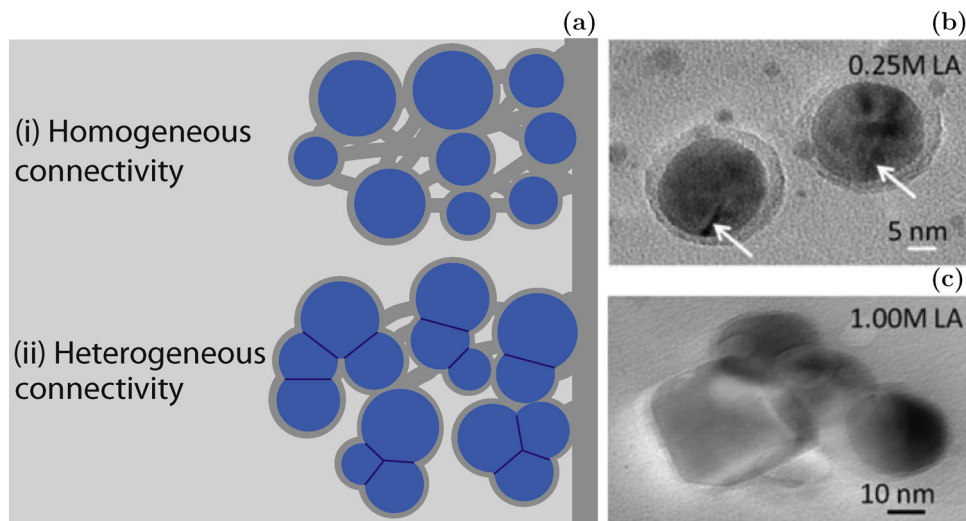


**Fig. 1.** (a) Schematics of two different possible Li redistribution mechanisms: (i) In the case with homogeneous connectivity, Li is transported through the electrolyte (and electrons through conductive carbon black or carbon-coating) to be redistributed from one particle to another. (ii) In the case with heterogeneous connectivity, Li can be directly transported between abutting particles. The electrostatic potential of the particles may become inhomogeneous due to poor electronic connectivity, which is not considered here. (b) TEM image of a sample where the particles are perfectly coated and not in direct contact between each other corresponding to case (i). (c) TEM image of particles in possible direct contact between each other, corresponding to case (ii). Figures (b) and (c) are reproduced with permission from Ref. 51, copyright 2011, Cambridge University Press.

(LFP) electrodes, non-bulk thermodynamics [57,58] or kinetics [5,6–8] may prevent the phase-separation from occurring inside the particle (*i.e.*, “intraparticle phase separation”). Instead, Li is redistributed between nanoparticles so they can reach their stable phases without having the energy penalty of forming an interface (*i.e.*, they undergo “interparticle phase separation” [5]). Given the driving force toward interparticle phase separation and a network of active particles in which Li can be redistributed, particles transform sequentially in the slow (dis)charging limit [2]. Thus, at any given time, a small fraction of the particles in the electrode sustains the entire current of the cell. Consequently, the cell voltage does not translate easily into the SOC of the active particles, as it also depends on additional factors such as charge and discharge history [9], particle size distribution, and cathode architecture (which determines how the particles are connected to other particles) [4,10].

Interparticle Li redistribution has been experimentally verified in LFP nanoparticles [11]. However, how this process occurs *in situ* during battery operation has remained unaddressed in the literature and is the central subject of this study. Specifically, the dependence of the process on the connectivities (both ionic and electronic) between particles is an important design consideration [4,12], which has not been studied in detail. In this work, we provide new insights on the Li redistribution and its dependence on architecture that help explain the following experimental observations. First, LFP electrodes have been shown to charge and discharge very inhomogeneously at the many-particle scale in several *in situ* experiments. In these experiments, a discrepancy is observed between the electrochemical measurements, representing the overall state of the cell, and spectroscopic data, indicating the local state [13,14]. Second, fully lithiated and fully delithiated particles have been observed to coexist in *ex situ* characterization of partially charged LFP [15,16]. Third, a notable spread in cycling performance occurs with varying electrode architecture and preparation.

In this paper, we present a model of the interparticle dynamics during operation in an electrode consisting of many active monophasic nanoparticles of a host material that, when in equilibrium, thermodynamically favors phase separation (*i.e.*, particles in a non-equilibrium solid solution). With an eye toward both understanding the dominant mechanisms that contribute to

inhomogeneous (dis)charging at the electrode scale and identifying practical methods to address them, we develop a model that describes Li redistribution between particles during the (dis)charge process in two different electrode architectures. These two architectures correspond to nanoparticle agglomerates (often observed in nanoparticulate electrodes [17–19]) of different densities: a dilute agglomerate and a dense agglomerate. These two constructions are illustrated in Fig. 1(a). The first architecture (Fig. 1(a)(i)) consists of active particles coated and “wired” with electronically and ionically conducting material, providing excellent electrical connectivity to the current collector and ionic connectivity to the electrolyte. Furthermore, the coating prevents any direct contact among active particles. This architecture is hereafter referred to as the configuration with “homogeneous connectivity.” In the second architecture (Fig. 1(a)(ii)), no or partial coating/wiring leads to direct contacts of active particles in clusters, which provides an additional path for Li transport. In addition, electrical and ionic connectivities are reduced and the electrostatic potential of the particles may become inhomogeneous (the consequence of which is not considered here as discussed later). This architecture is referred to as the configuration with “heterogeneous connectivity.” Similar to the work of Kang and Ceder [20], the nanoparticles considered here have an average size (diameter) of ~50 nm. We choose simulation parameters specific to simulate (dis)charging a network of different-size LFP nanoparticles, a commercial cathode material known for both its high-rate performance [21,20,22] and its thermodynamic tendency to phase separate [23,24].

## 2. Theory and Background

The inhomogeneous charge and discharge processes studied in this work result from the contributions of two mechanisms: (1) a non-monotonically decreasing single-particle equilibrium potential with respect to lithium uptake ( $\phi_{eq}$  vs.  $C_p$ ), characteristic of a phase separating material, and (2) the ability to redistribute Li between active particles. Although the multi-particle equilibrium defined here has been thoroughly studied recently in the literature [2,25], our model additionally takes into account the connectivity between the particles and their interaction during Li (de)insertion,

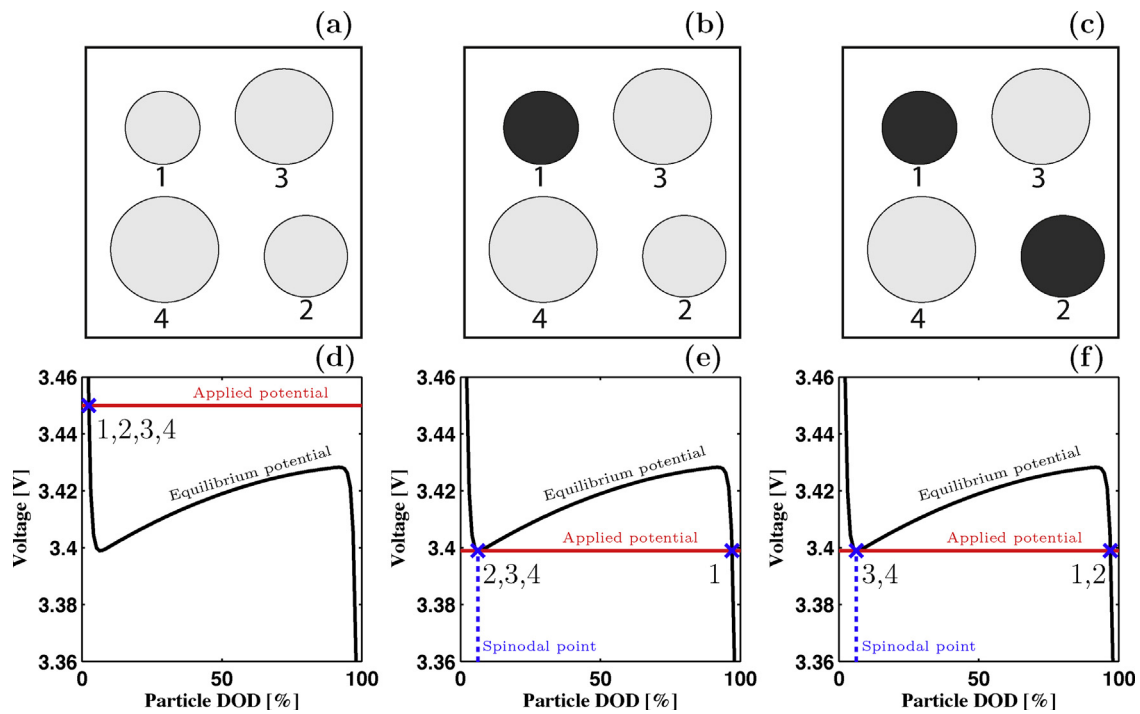


**Fig. 2.** Schematic of the sequential transformation of four particles in the case where interparticle exchange is ignored, based on schematic from Ref. 4 (assuming the applied potential approximates the local potential difference across the particle-electrolyte interface,  $\Delta\phi$ ). (a), (b) and (c) represent the particles during their lithiation (the grayscale indicates the degree of lithiation; darker gray indicates higher Li concentration); (d), (e) and (f) indicate the applied voltage and the depth of discharge (DOD=1-SOC) of the particles. (a) & (d) At the beginning of the process, the voltage is constantly lowered to lithiate the particles. (b) & (e) When particles reach the spinodal point, the particles start lithiating sequentially due to the increasing driving force they gain due to the non-monotonic shape of the equilibrium potential. (c) & (f) The process continues until all particles are fully transformed.

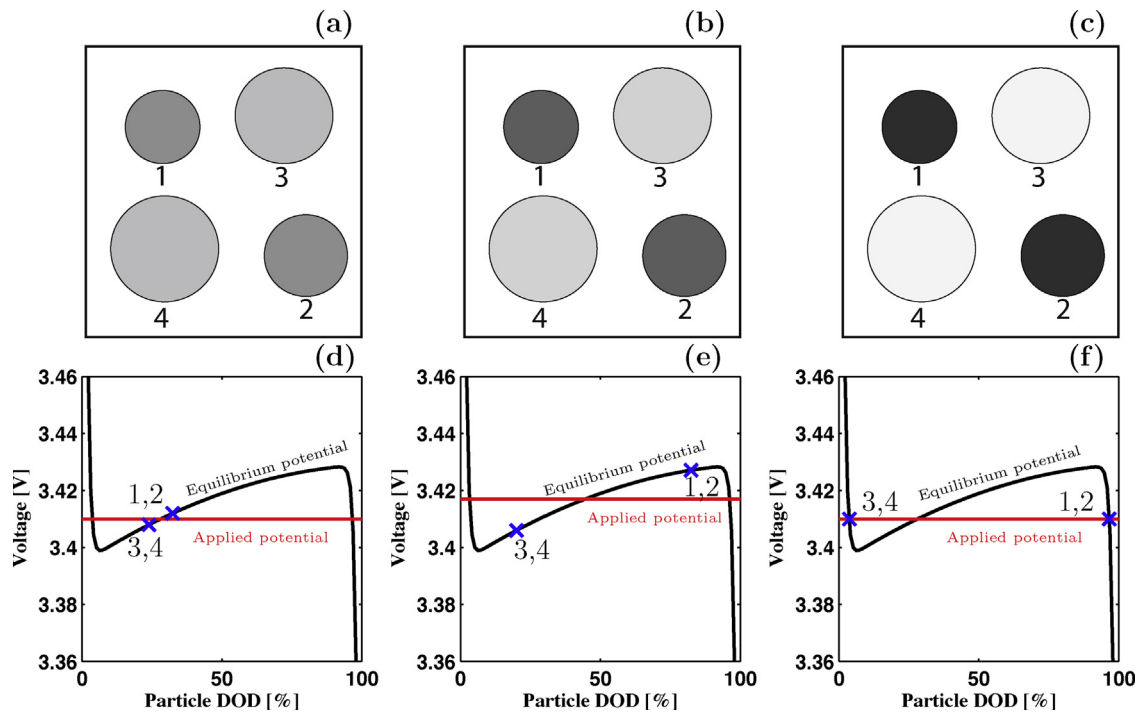


**Fig. 3.** Schematic of the Li redistribution between four particles via a reaction (assuming the applied potential approximates  $\Delta\phi$ ). (a), (b) and (c) represent the particles during the process (the grayscale indicates the degree of lithiation; darker gray indicates higher Li concentration); (d), (e) and (f) indicate the applied voltage and the DOD of the particles. (a) & (d) A small difference in the concentration determines which particles extract Li and which ones absorb Li. (b) & (e) While the redistribution occurs, the applied voltage fluctuates in order to equilibrate the insertion and the extraction. (c) & (f) The process finishes when the particles reach equilibrium at a Li-poor or a Li-rich phase.

to provide a physical understanding of the dynamics within the electrode as a function of the imposed discharge rate.

The two aforementioned mechanisms are now described in detail. The kinetics of Li insertion in an isolated active particle is governed solely by the non-monotonic shape of the equilibrium potential with respect to Li concentration [5]. Upon discharge, the applied potential across the cell is continually lowered to drive Li insertion, and the driving force for insertion is proportional to the difference between the applied potential and the equilibrium potential [4]. Therefore, due to the non-monotonic nature of the equilibrium potential with respect to Li uptake, beyond a specific Li concentration (the lower spinodal point) the driving force for additional Li insertion begins to increase, which accelerates the process. To clearly elucidate this process, we use Fig. 2 as a schematic illustration, in which the interparticle Li redistribution is ignored. We observe in Fig. 2(d) the initial voltage, which is lowered until reaching the voltage value corresponding to the spinodal point (Fig. 2(e)). At this concentration, particles transform sequentially (Figs. 2(e) and (f)). In a realistic electrode with many active particles interacting with each other, there is an additional driving force for interparticle Li redistribution to consider, which is driven by the reduction in free energy that is achieved by the transformation from particles at an intermediate Li concentration to a combination of Li-rich and Li-poor particles. This process is illustrated in Fig. 3, where four particles with an intermediate concentration reach equilibrium by exchanging Li with each other. The redistribution of Li amongst particles is triggered when some particles begin undergoing accelerated lithiation causing a rise in the voltage. This increase in the voltage causes a driving force for the particles not undergoing fast lithiation to delithiate. Thus, particles extract or absorb Li (from each other) and tend to transform to a Li-poor or a Li-rich phase. Some incubation time is required before the next redistribution of Li can be triggered, as the delithiated particles need to absorb enough Li to be able to return to the spinodal point and trigger the next instability [26]. This causes an intermittent phase transformation that leads to group-by-group lithiation of particles of similar sizes.

To elucidate the contribution associated with the connectivity of the particles, we consider two separate cell architectures. First, we investigate a dilute configuration with homogeneous connectivity. This corresponds to an idealized electrode configuration where the particles are completely separated from each other by embedded electronic conductors. In this case, Li can only be redistributed via a reaction by which the resulting ionic Li and electrons are transported through the electrolyte and the electronic conductors, respectively. As it will be shown later, in this ideal case, the lithiation/delithiation processes of individual particles are nearly independent of their position with respect to other particles, as well as the separator and current collector. This is because the salt concentration in the electrolyte is nearly constant throughout the small domain considered here ( $\sim 300\text{ nm}$  in length) due to the fast Li-ion transport in the electrolyte and the relatively high porosity of the two cell constructions. Fig. 1(a)(i) shows a schematic representation of this architecture and Fig. 1(b) a transmission electron microscopy (TEM) image of well-spaced particles. Second, we analyze a configuration with heterogeneous connectivity, a more realistic electrode configuration representative of a dense agglomerate of particles. In heterogeneously connected particles, there is a spatial preference in the order of reaction of the particles caused by the direct contact between particles and electrostatic potential inhomogeneities. Here, we model the heterogeneous connectivity solely by the direct transport between particles. Explicitly tracking the electronic conductors network and solving for the electrostatic potential of the conductors and particles is beyond the scope of this work. However, it is important to note that inhomogeneities in the voltage would lead to more

inhomogeneity in the lithiation of the particles than what we report here. Fig. 1(a)(ii) shows a schematic representation of the configuration with heterogeneous connectivity and Fig. 1(c) a TEM image of heterogeneously connected particles. The direct contact between the particles facilitates a redistribution of Li via the contact area, driven simply by a transport process (dependent on the chemical potential difference between the contacting particles) through a permeable boundary. In this configuration the dynamics is “local-environment dependent” because contacting particles are strongly coupled through direct transport rather than the weaker electrochemical interactions. The direct transport can be physically interpreted as a “shortcut” path because it allows Li to move from one particle to another without an electrochemical reaction.

Direct Li transport between LFP particles has not been studied before in the literature as a mechanism for Li redistribution. However, there is substantial evidence for its existence via analyzing the ionic conductivity of electrode constructions of bare pristine LFP (without electrolyte nor additives). For example, in the work of Wang and Hong [27], the ionic conductivity of a pristine LFP cathode was measured to be in the range of  $10^{-5}\text{ S/cm}$  (equivalent to an ionic diffusivity of  $10^{-10}\text{ cm}^2/\text{s}$ ). In such constructions, the Li transport in the cathode is limited to the direct Li transport between the particles, as there is no driving force for electrochemical reactions.

### 3. Model

#### 3.1. Governing Equations

To describe the governing physics of an electrochemical cell, we employ four coupled equations: concentration evolution in the (1) cathode particles and (2) electrolyte, (3) current continuity in the electrolyte (for the sake of simplicity we assume that the electric potential within cathode particles is uniform), and (4) reaction at the electrode-electrolyte interface. Concentration evolution in the cathode particles is described by Fickian diffusion to approximate non-equilibrium solid-solution Li diffusion [5],

$$\frac{\partial C_p}{\partial t} = \nabla \cdot (D_p \nabla C_p) \in V_p, \quad (1)$$

where  $C_p$  is the concentration of Li in the particle,  $t$  is time,  $D_p$  is the diffusion coefficient in the particle, and  $V_p$  is the bulk region of the particles. For the concentration evolution of the salt in the electrolyte, the dilute binary solution theory is used [28]:

$$\frac{\partial C_e}{\partial t} = \nabla \cdot (D_{amb} \nabla C_e) - \frac{\mathbf{i} \cdot \nabla t_+}{z_+ v_+ F} \in V_e, \quad (2)$$

where  $C_e$  is the salt concentration in the electrolyte,  $D_{amb}$  is the ambipolar diffusion coefficient,  $\mathbf{i}$  is the current density vector,  $F$  is Faraday's constant, and  $V_e$  is the bulk of the electrolyte. Furthermore,  $t_+$ ,  $z_+$ , and  $v_+$  are the transference, charge, and dissociation numbers of the cation, respectively. We assume the electrolyte is electroneutral and therefore its electrostatic potential can be described using the charge conservation principle:

$$\nabla \cdot \left[ \frac{F}{RT} (z_+ D_+ - z_- D_-) C_e \nabla \phi_e \right] + \nabla \cdot [(D_+ - D_-) \nabla C_e] = - \frac{\nabla \cdot \mathbf{i}}{z_+ v_+ F} \\ = 0 \in V_e, \quad (3)$$

where  $R$  is the ideal gas constant,  $T$  is the absolute temperature,  $\phi_e$  is the electrolyte electrostatic potential,  $z_-$  is the charge number of the anion, and  $D_j$  is the diffusion coefficient of ionic species  $j$ . This approximation assumes thin double layers, which is adequate for electrolytes where no depletion occurs [7]. (For models accounting for double-layers/non-neutral electrolytes see Refs. 29 and 30.) The Butler-Volmer equation is used to model the electrochemical reaction assumed to take place at the particle-electrolyte

interface (as commonly implemented in LFP [31,8,26] and other battery materials [32,33] simulations),

$$r_{Li} = \frac{i_0}{F} \sqrt{\frac{C_e}{C_e^0}} [\exp(-\frac{\alpha F}{RT} \eta) - \exp(\frac{(1-\alpha)F}{RT} \eta)], \quad (4)$$

where  $r_{Li}$  is the reaction rate,  $i_0$  is the exchange current density,  $\alpha$  is the transfer coefficient,  $\eta$  is the overpotential at the particle-electrolyte interface, and  $C_e^0$  is the concentration at which  $i_0$  is experimentally measured. For simplicity, we here assume  $i_0$  is independent of the cathode concentration. The overpotential is defined as  $\eta = \Delta\phi - \phi_{eq}$ , where  $\Delta\phi = \phi_p - \phi_e$ , and  $\phi_p$  is the particle electrostatic potential. The single-particle equilibrium potential,  $\phi_{eq}$ , is defined as  $\phi_{eq} = V_{OC} - \mu/F$  [7,26], where  $V_{OC}$  is a reference value at a measured open circuit voltage plateau [34] and  $\mu$  is the chemical potential, obtained from a first principles calculation [5]. The polynomial used to define the chemical potential is

$$-\mu/F = \{[5(1.05 - 2.1x)^{51} - 2.925275x^2 + 6.375071x - 2.558325] \times 10^{-2}\} [V], \quad (5)$$

where  $x$  corresponds to the site fraction of Li in  $\text{Li}_x\text{FePO}_4$ . The overpotentials that are observed in our simulations are well within the regime in which the Butler-Volmer kinetics provides a good approximation for the reaction kinetics – even at the highest rate, the overpotential is only slightly over the 100 mV boundary, where the Butler-Volmer kinetics begins to differ from the Marcus-Hush-Chidsey kinetics [35,36].

Three boundary conditions are used for the concentration evolution in the particles (Eq. (1)). On the particle-electrolyte interface,  $A_r$ ,

$$\vec{n}_e \cdot \mathbf{J} = r_{Li} \in A_r, \quad (6)$$

where  $\vec{n}_e$  is the unit normal vector of the electrolyte-particle interface pointing inward to the particle, and  $\mathbf{J}$  is the interfacial flux. At the particle-particle boundary,  $A_p$ , present only in the dense agglomerate, the boundary condition is

$$\vec{n}_p^{i,j} \cdot \mathbf{J} = \frac{\rho}{RT} P(\mu_j - \mu_i) \in A_p, \quad (7)$$

where  $\vec{n}_p^{i,j}$  is the unit normal vector from particle  $j$  to particle  $i$  at the contact interface,  $\rho$  is the interstitial site density,  $P$  is the permeability of the interface, and  $\mu_i$  and  $\mu_j$  are the chemical potentials of the two particles in contact. Periodic boundary conditions are assumed in the box boundaries.

The boundary conditions for the two fields in the electrolyte are the following. For the salt concentration (Eq. (2)), the boundary condition on the particle-electrolyte interface is [7],

$$\vec{n}_e \cdot \mathbf{J} = -(1 - t_+) r_{Li} \in A_r, \quad (8)$$

and a flux boundary condition is imposed at the anode-electrolyte interface,  $A_A$ . The flux is defined as

$$\vec{n}_a \cdot \mathbf{J}|_{A_A} = \frac{1}{S_A} \int_{A_r} (1 - t_+) r_{Li} dA, \quad (9)$$

where  $\vec{n}_a$  is the unit normal vector pointing inward to the electrolyte and  $S_A$  is the total surface area of the anode-electrolyte interface. For the charge conservation principle (Eq. (3)), the divergence of the current is proportional to the reaction flux,

$$-\frac{\nabla \cdot \mathbf{i}}{z_+ \mathcal{U}_+ F} = \frac{r_{Li}}{\nu_+} \in A_r. \quad (10)$$

The electrostatic potential at the anode-electrolyte interface is set at 0 V. For both the electrostatic potential and the salt concentration of the electrolyte, no flux boundary condition is used at the electrolyte-current collector interface, and periodic boundary conditions are used on the remaining box boundaries.

In order to focus on the dynamics of particles within the cathode, we consider pure Li metal to be the reference anode, which is not explicitly tracked. Because of the small size of the electrochemical cells considered here, the gradients in the electrostatic potential and salt concentration of the electrolyte are small and therefore we do not describe those results. For the same reason, we express the observed dynamics in terms of the applied voltage of the cell instead of the local potential difference across the interface ( $\Delta\phi$ ) as these two values are fairly similar. Our model is general, and can be used for charge and discharge. However, for convenience, in this work we only show the results of discharging a cell.

### 3.2. Smoothed Boundary Method

To circumvent the tedious structural meshing in conventional numerical methods, we employ the smoothed boundary method (SBM) [37] to reformulate the partial differential equations (PDEs) describing the electrochemical dynamics. In the SBM, a continuous parameter is used to indicate the different domains. The domain parameter,  $\psi_T$ , is of a uniform value in one phase (representing the bulk), and transitions from one domain to another in a very narrow region (representing a boundary). In this work, we set  $\psi_T = 1$  in the cathode particles, and  $\psi_T = 0$  in the electrolyte. The particle-electrolyte interface is indicated by  $0 < \psi_T < 1$ , where the smooth transition of the domain parameter is created using a hyperbolic tangent function [37]. By defining different phases with the values of the domain parameter, one can conveniently solve different governing equations for problems with multiple phases. For the dilute agglomerate, the 65 particles were defined using  $\psi_{i=1} = \psi_T$ . Alternatively, for the dense agglomerate the 200 particles were described by five domain parameters such that neighboring particles are defined by distinct domain parameters,  $\psi_i$ , where  $i = 1$  to 5. The sum of  $\psi_i$  is equal to  $\psi_T$ .

The SBM formulation of our governing equations is given below. For the dilute agglomerate, only one concentration variable,  $C_{p,i=1}$ , was used to represent the concentration of Li in the particles since there is only one domain parameter for the particles in this case. For the dense agglomerate, five concentration variables,  $C_{p,i}$ , were evolved with their corresponding domain parameters, according to

$$\begin{aligned} \frac{\partial C_{p,i}}{\partial t} = & \frac{D_p}{\psi_i} [\nabla \cdot \psi_i \nabla C_p] + W_{r,i} \frac{|\nabla \psi_i|}{\psi_i} r_{Li,i} \\ & + \sum_{j \neq i} W_{p,i} \frac{|\nabla \psi_i|}{\psi_i} \frac{\rho}{RT} P(\mu_j - \mu_i), \end{aligned} \quad (11)$$

which combines Eq. (1) with the two boundary conditions for reaction (Eq. (6)) and interparticle flux (Eq. (7)). Here,  $r_{Li,i}$  is the reaction rate for particle  $i$ ,  $W_{r,i}$  and  $W_{p,i}$  are the weighting factors [37] for reaction and interparticle flux, respectively, which are defined as

$$W_{r,i} = \left( \frac{|\nabla \psi_i| |\nabla \psi_T|}{\sum_{j=1}^n \sum_{k=j+1}^n |\nabla \psi_j| |\nabla \psi_k| + \sum_{j=1}^n |\nabla \psi_j| |\nabla \psi_T|} \right)^\beta, \quad (12)$$

$$W_{p,i} = \left( \frac{\sum_{j \neq i} |\nabla \psi_i| |\nabla \psi_j|}{\sum_{j=1}^n \sum_{k=j+1}^n |\nabla \psi_j| |\nabla \psi_k| + \sum_{j=1}^n |\nabla \psi_j| |\nabla \psi_T|} \right)^\beta, \quad (13)$$

where  $n$  is the number of domain parameters and  $\beta$  is the weighting factor exponent [37]. These weighting factors identify the two types of boundaries: the particle-electrolyte boundary and the particle-particle boundary. Note that in the case of the dilute electrode, the third term on the right hand side of Eq. (11) vanishes, and  $W_{r,i} = 1$  at all electrolyte-particle interfaces. For the salt concentration

evolution in the electrolyte, Eq. (2) is reformulated with its boundary condition (Eq. (8)) to [26]

$$\frac{\partial C_e}{\partial t} = \frac{D_{amb}}{1 - \psi_T} [\nabla \cdot ((1 - \psi_T) \nabla C_e)] - (1 - t_+) \sum_{i=1}^n W_{r,i} \frac{|\nabla \psi_i|}{1 - \psi_T} r_{Li,i}, \quad (14)$$

where the electrolyte domain is represented by  $1 - \psi_T = 1$ . Equation (3) is reformulated with the boundary condition shown in Eq. (10) to [26]

$$\begin{aligned} & \nabla \cdot [(1 - \psi_T) \frac{F}{RT} (z_+ D_+ - z_- D_-) C_e \nabla \phi_e] \\ &= \sum_{i=1}^n W_{r,i} |\nabla \psi_i| \frac{r_{Li,i}}{\nu_+} + \nabla \cdot [(1 - \psi_T) (D_- - D_+) \nabla C_e]. \end{aligned} \quad (15)$$

Note that  $D_p$ ,  $D_+$ , and  $D_-$  were assumed constant in this work.

### 3.3. Parameters and Numerical Methods

The parameters employed in the simulations are summarized below. The diffusivities of Li in the particles and of the salt in the electrolyte are assumed constant. In the particles, Li diffusivity is set to be  $D_p = 5 \times 10^{-13} \text{ cm}^2/\text{s}$ , which is comparable to those found in literature [38,39]. While larger values have also been reported [40,41],  $D_p$  here is large enough to result in a nearly uniform Li concentration within the cathode particles at the applied currents imposed in this study, and thus, the results would not depend significantly on this parameter. We take the solution of LiPF<sub>6</sub> salt in a propylene carbonate solvent as the electrolyte, where the diffusivities of the ions are taken to be  $D_+ = 7.3 \times 10^{-7} \text{ cm}^2/\text{s}$  and  $D_- = 1.5 \times 10^{-6} \text{ cm}^2/\text{s}$  for Li<sup>+</sup> and PF<sub>6</sub><sup>-</sup>, respectively. These values of the ionic diffusivities were measured for the electrolyte at a concentration of 1 M (mol/L) [42], which is the average salt concentration of the electrolyte. We take the permeability of the particle-particle interface,  $P$ , to be the conservative value of  $1 \times 10^{-7} \text{ cm/s}$ . This value is equivalent to  $5 \times 10^{-14} \text{ cm}^2/\text{s}$  if an interfacial thickness of 5 nm is assumed, and it is approximately one order of magnitude smaller than the bulk diffusivity of the particle. Simulations are performed for a temperature,  $T$ , of 300 K. The site density,  $\rho$ , is estimated from the lattice constants to be 0.0228 mol/cm<sup>3</sup> [43], and  $V_{OC}$  of 3.42 V is adopted from an experimental value [34]. The exchange current density,  $i_0$ , is set to  $8.5 \times 10^{-7} \text{ A/cm}^2$ . This value was obtained by scaling the experimentally obtained value [44] by a factor of 200 in order to account for the difference between the actual particle surface area and the macroscopic cathode surface area at which it was measured [6]. For the electrostatic potential, as mentioned earlier, we assume that it is uniform throughout the particles. The value of 0.8 is used for  $\beta$  appearing in the weighing factors, which is a numerical parameter that represents processes near three-phase boundaries optimally [37].

A central finite difference scheme is employed for spatial discretization, where  $\Delta x = 2.5 \text{ nm}$ . A fully implicit time stepping scheme is used to update the salt concentration, Eq. (14), using the alternating-direction-line-relaxation method [45,46,37]. The electrostatic potential in the liquid, Eq. (15), is also solved by the alternating-direction-line-relaxation method. An Euler explicit time stepping scheme is employed with Eq. (11) for the concentration field in the particles.

## 4. Results

We simulate the electrochemical process based on two configurations: a “dilute” electrode and a “dense” electrode. These configurations represent the case of homogeneously and heterogeneously connected particles, respectively. We present the results for the dilute electrode, followed by the results for the dense electrode. An analysis for both configurations is then presented. The

simulation configurations were chosen to facilitate comparison to experimental measurements of LFP composite electrodes.

### 4.1. Dilute Electrode (With Homogeneous Connectivity)

The dilute electrode is an idealized scenario with optimal ionic and electronic connectivity. It consists of 65 particles in a  $320 \times 320 \times 300 \text{ nm}^3$  volume with a region without particles of approximately 30 nm placed at the bottom, which corresponds to the separator. The configuration is depicted in Fig. 4. This agglomerate has a volume fraction of 22% active particles. We assume a log-normal distribution of the particle radii shifted by  $b$ , namely with a probability density function:

$$f_{a,\sigma,b,\beta}(r) = \begin{cases} \frac{1}{\sigma(r-b)\sqrt{2\pi}} \exp\left(-\frac{[\ln((r-b)/\beta)-a]^2}{2\sigma^2}\right) & \text{if } r > b \\ 0 & \text{if } r \leq b, \end{cases} \quad (16)$$

where  $r$  is the particle radius (in nanometers),  $a = 1$ ,  $\sigma = 0.2$ ,  $b = 5 \text{ nm}$ , and  $\beta = 7.5 \text{ nm}$ . The radii of the particles obtained are in the approximate range from 18.7 nm to 35 nm. Results from the dilute electrode simulations serve two purposes. The first is to remove the effect of the heterogeneous connectivity to gain a general understanding of the lithiation of a multi-particle assembly of phase-separating active particles. Secondly, this configuration serves as the ideal case in terms of the electrode performance as will be shown later.

Fig. 4 illustrates how lithiation proceeds in a dilute electrode at the lowest rate of discharge considered (C/11.1 rate) at three different snapshots with respect to cell depth of discharge (DOD=1-SOC). As previously mentioned, during the cathode lithiation, two distinct processes occur simultaneously within the cathode: a constant flux of Li ions into the cell and Li redistribution amongst active particles. The snapshots highlight that the majority of the particles are in either a Li-rich or a Li-poor state during the entire process, and only a small population of the particles is at an intermediate concentration at any time. For instance, Particle A (highlighted in Fig. 4(d)) is nearly fully delithiated when the cell is at 43% DOD but is nearly fully lithiated by the time the cell is at 71% DOD, and Particle B is nearly fully lithiated by 43% DOD. The inhomogeneous lithiation of the particles observed at this current is caused by the Li redistribution between particles, which is more rapid than the overall lithiation of the cell. There is no obvious spatial dependence as to which particles transform in which order, but there is an obvious size-dependent correlation as seen in Fig. 5.

The Li content across the entire particle size distribution is shown as a function of cell discharge (at three increasing discharge rates) in Figs. 5(a)–(c). Particles are ordered from smallest to largest along the y-axis, the x-axis is the cell DOD, and the color indicates the DOD of the individual particles. The Li concentration evolution in two randomly chosen particles (labeled Particle A and Particle B in Fig. 4(d)) is shown in Figs. 5(d)–(f). The overall trend, regardless of rate, is that smaller particles transform before larger ones. This is caused by the larger surface area to volume ratio of the smaller particles as Li intake is proportional to the area, and the particle capacity is proportional to the volume. Thus, the smaller particles reach the concentration instability (or spinodal point) that accelerates further Li insertion into the particle before the larger particles. (Note that the tendency for smaller particles to lithiate before larger ones would be reinforced if the equilibrium potential were assumed to be particle-size dependent [47,48].)

In the zero current limit, it has been proposed that discharging an assembly of particles with a non-monotonic single-particle equilibrium potential results in discrete (sequential) transformation [2]. On the other hand, in the high-rate limit, the magnitude of

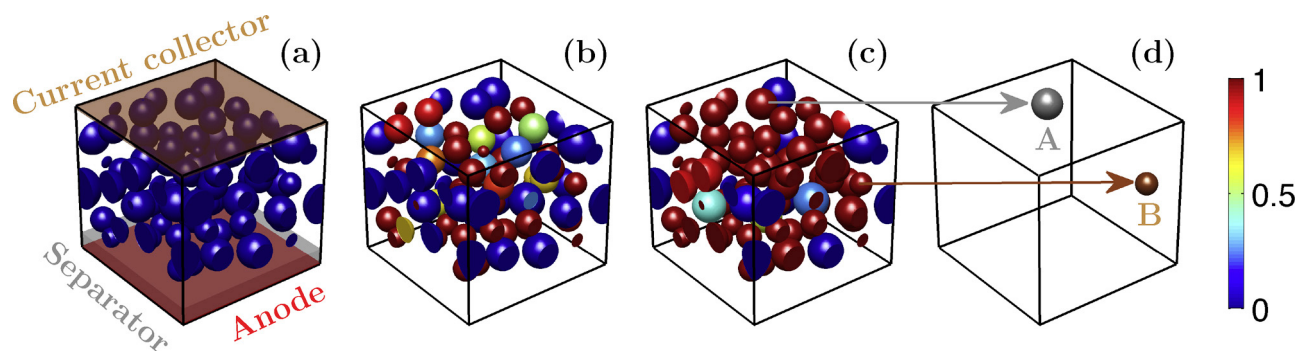


**Fig. 4.** Li lattice-site-fraction ( $0 = \text{FePO}_4$ ,  $1 = \text{LiFePO}_4$ ) in the dilute agglomerate formed by 65 particles plotted here during discharge at C/11.1 rate. (a) Initial concentration, 2% cell DOD. (b) At 43% cell DOD. (c) At 71% cell DOD. (d) Two randomly selected particles labeled as Particle A and Particle B used for discussion in the text. In (a) the location of the cathode current collector, separator and anode are indicated.

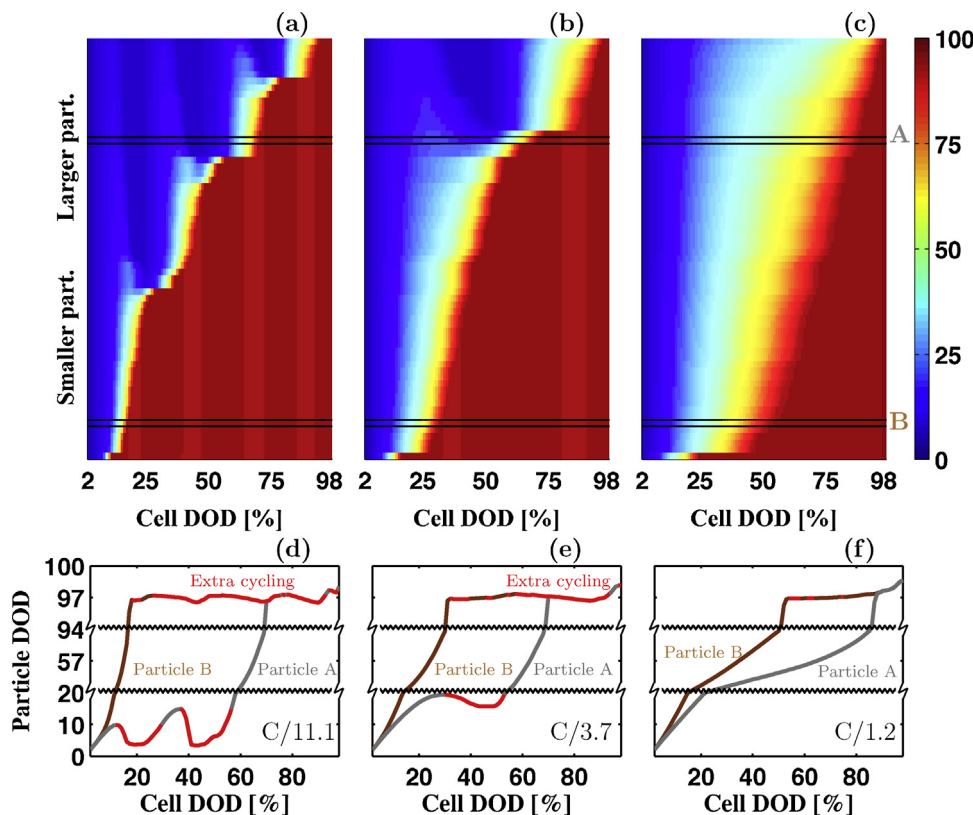


**Fig. 5.** (a)–(c) DOD of the particles during discharge arranged from smaller diameter to larger (a) at C/11.1 rate, (b) at C/3.7 rate, and (c) at C/1.2 rate. The color indicates the DOD of the particles from blue (fully delithiated) to red (fully lithiated) as shown in the color bar. (d)–(f) Particle A and particle B during discharge at the same three C-rates. The red portion of the curves indicates the partial delithiation/re-lithiation cycles caused by the particles interactions. The delithiation events seen in (f) are very small and undetectable in this figure (but are noted in red). Note that the y-axis in (d)–(f) is not in linear scale.

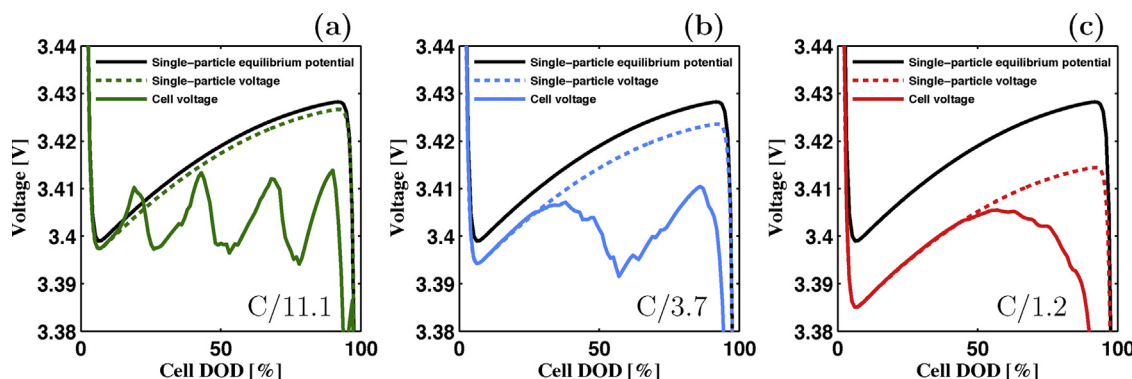


**Fig. 6.** Cell voltage (colored solid line) during the discharge of the dilute electrode at (a) C/11.1, (b) C/3.7, and (c) C/1.2 rates. For comparison, the single-particle equilibrium potential (solid black line) and the potential of a single average-size particle would experience at the same rate (dashed colored line, see text) are also plotted.

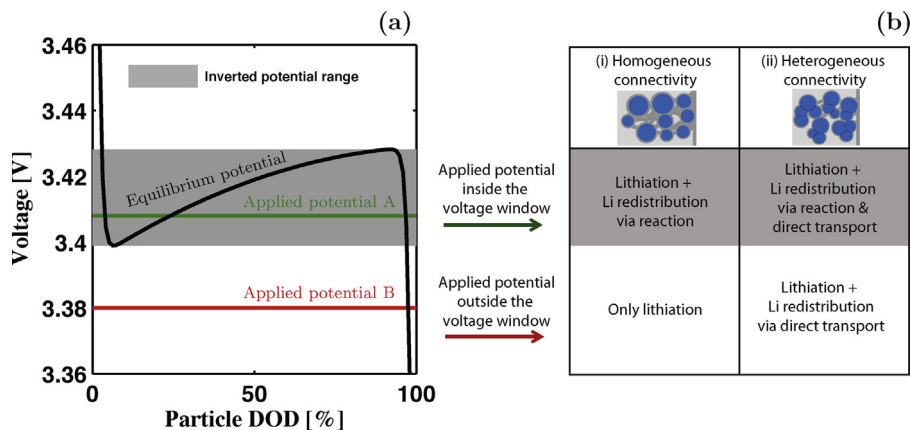


**Fig. 7.** (a) Schematic of the applied potential for different scenarios during cell discharge. (b) Cell behaviors observed (assuming the applied potential approximates  $\Delta\phi$ ). (i) For homogeneously connected particles, redistribution via reaction only occurs when the applied voltage is inside the inverted potential range (applied potential A). When the applied potential is outside the inverted potential range (applied potential B), only lithiation can occur. (ii) For heterogeneously connected particles, additionally, redistribution via direct transport can occur at any current.

the applied potential exceeds the difference between the values of the equilibrium potential corresponding to the two concentration instability points, and thus Li insertion would be homogeneously distributed amongst all particles assuming uniform electrostatic potential [4,6]. In Fig. 5(a)–(c), the transition between these two limits can be clearly seen. At the lowest rate, lithiation proceeds group-by-group as observed in Fig. 5(a), where there are clearly four groups that transform in sequence. At intermediate rate, shown in Fig. 5(b), there are two identifiable groups transforming sequentially, and at higher rates (Fig. 5(c)) most of particles transform simultaneously (although smaller particles still transform first). Therefore, as the discharge rate is reduced, the fraction of particles concurrently involved in phase transformation becomes smaller. Consequently, the entire current of the cell must be sustained by a smaller fraction of the particles in the cell. This notion is opposite of what is understood for solid solution systems where the distribution of current over the cell would be homogenized by decreasing the discharge rate.

Several particles exhibit non-monotonic lithiation behavior, partially delithiating before re-lithiating during the course of a single cell discharge, as observed in Figs. 5(d)–(f) for Particle A and Particle B. Depending on the rate, each particle within the cell may undergo multiple (partial) delithiation/re-lithiation cycles within a single cycle of a cell, resulting in a significantly higher local rate. Thus, the lithiation process of individual particles is very different from the average across the entire cell. For instance, Particle A in Fig. 5(d) (C/11.1 rate) undergoes two Li concentration fluctuations, the first at a cell DOD of  $\sim 20\%$  in which the particle delithiates approximately 6%, and the second at  $\sim 40\%$  DOD, in which the particle delithiates approximately 11%. Particle A, for example, undergoes an additional  $\sim 0.17$  cycle (highlighted in red). The amplitude of the oscillation of the particle DOD is larger when the particles are near the lower spinodal, while the concentration of the particles remains nearly constant when the particles are nearly fully lithiated. At higher rates, however, the effects of inter-particle Li transport and interparticle phase separation become negligible as homogeneous Li insertion dominates (as discussed earlier). Accordingly, Particle A and Particle B undergo less (partial) delithiation/re-lithiation cycles (*i.e.*, fewer and smaller red regions in Figs. 5(e)–(f) than in Fig. 5(d) as well as smaller associated concentration drop).

In Fig. 6, the cell voltage curve is shown at three different discharge rates along with the single-particle equilibrium potential (solid black curve) and the “single-particle voltage” (dashed curve) superimposed for comparison. The single-particle voltage

describes the behavior of an average-size single particle discharging at the same rate. It represents an unphysical scenario where the particles are identical, and are perfectly connected to the counter-electrode (ionically) and to the current collector (electrically) but *not* to other particles, which prevents the system’s free energy from reducing through interparticle Li redistribution. This curve illustrates the scenario where all particles transform simultaneously and independently. Consequently, the characteristic flat voltage profile associated with LFP electrodes is not observed in this scenario, and only when interparticle phase-separation occurs (*i.e.*, through interparticle Li redistribution) a voltage plateau emerges. At C/11.1 rate (Fig. 6(a)), the voltage curve strongly resembles the multi-particle equilibrium curve described by Dreyer *et al.* [2] in which all particles are either nearly fully lithiated or delithiated. In this case, there are four distinct undulations in the voltage, which correspond to the four groups of particles transforming in sequence as described earlier, with regions of decreasing voltage corresponding to the interparticle phase separation. As rate increases, the number of undulations (and therefore the number of groups of particles) reduces. At C/3.7 (Fig. 6(b)), two undulations are observed, and at C/1.2 (Fig. 6(c)) all particles react in one group. At C/1.2, a larger overpotential is required to maintain the constant current, resulting in an increased deviation from the single-particle voltage, but as particles react concurrently, the shape of the curve appears similar to the single-particle voltage. In all the three cases, the difference between the cell and single-particle voltage curves arises from the combination of the effects of the size distribution and of the Li redistribution between particles.

The interactions in homogeneously connected particles occur only when the current is sufficiently low. As previously mentioned, in this type of connection, Li redistribution only occurs via an electrochemical reaction. Thus, redistribution is limited to the case when the applied potential falls between the local minimum and the local maximum of the equilibrium potential, referred hereafter as the “inverted potential range” (see Fig. 7(a)). As illustrated in Fig. 3, for significant redistribution to occur, some particles need to have a driving force to lithiate and some to delithiate, which can only occur in this region. Outside of the inverted potential range, all the particles have a driving force for lithiation (except for small concentration fluctuations, as shown in Fig. 5(f), noted by the red portions of the curve). When discharging the cell at C/11.1 and C/3.7, the applied potential falls inside the inverted potential range and thus significant redistribution is observed. However, when discharging at C/1.2, this is no longer the case for most of the process and the driving force for redistribution is no longer present.

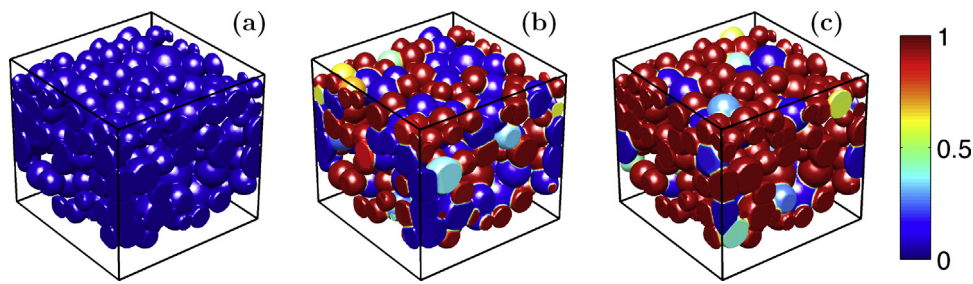


**Fig. 8.** Li lattice-fraction in the dense agglomerate composed of 200 particles plotted here during discharge at 1 C-rate. (a) Initial condition with cell DOD = 2%, (b) cell DOD = 43%, and (c) cell DOD = 71%.

A schematic of the different regimes for cell behavior in homogeneously connected particles is shown in Figs. 7(a) and (b)(i). Fig. 7(b) tabulates the cell behavior that is observed depending on whether the applied voltage is in or outside the inverted potential range.

As DOD increases, the cell potential deviates further from the single-particle voltage because, as some particles complete their transformation, fewer particles must sustain the same cell current density, effectively increasing the local rates. The particles react less uniformly due to the dispersion of the particle size. At C-rates at which the interactions are suppressed, it is more efficient to have a small dispersion in particle-sizes because the magnitude of the overpotential for all particles would be similar at all DODs. At lower currents, where Li redistribution occurs, the electrode should be designed to reduce interparticle Li redistribution since it is a dissipative mechanism that leads to energy loss, and the free energy reduction that results from interparticle phase separation decreases the efficiency of the cell.

#### 4.2. Dense Electrode (With Heterogeneous Connectivity)

As mentioned earlier, the dilute electrode configuration represents an idealized scenario where there is a homogeneous connectivity between active particles. To better understand the behavior of a more realistic electrode configuration, we introduce a dense agglomerate in which 200 particles are closely packed and in contact with each other, as shown in Fig. 8. In this cell, the volume fraction of active particles is 52%. The same simulation volume (for both the cathode and the separator) and particle size

distribution as in the dilute electrode are used. Here, we introduce an additional mechanism that facilitates Li redistribution between particles when they are in contact with each other (described in detail in the Model Section). Thus, this configuration corresponds to a heterogeneous network that better represents the electrode architecture of a realistic composite electrode in which agglomeration of nanoparticles results in particle-particle contacts.

Overall, increased particle density and preferential Li redistribution between neighboring particles leads to more sequential (discrete) lithiation for a given rate and generally poorer cell performance, as compared to the dilute configuration. In Fig. 8, the arrangement of Li within the cell is shown at three different snapshots in time during a single discharge cycle at 1C. The inhomogeneity in Li distribution across the cell is readily seen in Fig. 8(b), with the majority of particles either nearly fully lithiated or fully delithiated. This is similar to the case where the dilute electrode particles transform sequentially. However, in a dense agglomerate this behavior persists at higher rates. For instance, in the dilute electrode, the case with C/1.2 rate shows nearly simultaneous lithiation (Fig. 5(c)), while in the dense agglomerate sequential lithiation prevails at 1 C-rate. In the dilute electrode simulations, there is no obvious spatial dependence as to which particles transform after another. In these cases, the order of lithiation is controlled only by the particle size, which changes the surface area to volume ratio of a particle. However, in the dense agglomerate, the order of reaction depends on two factors: First is the ratio between active surface area (*i.e.*, particle-electrolyte interface) and volume of the particle. Second is the active surface area to volume ratio of neighboring

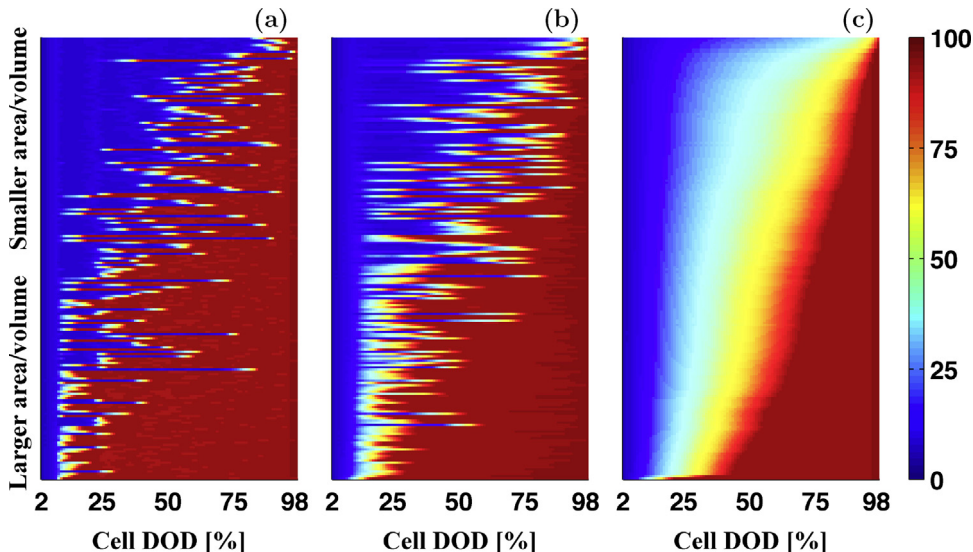


**Fig. 9.** DOD of the particles arranged by active surface area to volume ratio during discharge. At (a) 1C and (b) 10C with heterogeneous connectivity. (c) At 1C with homogeneous connectivity.

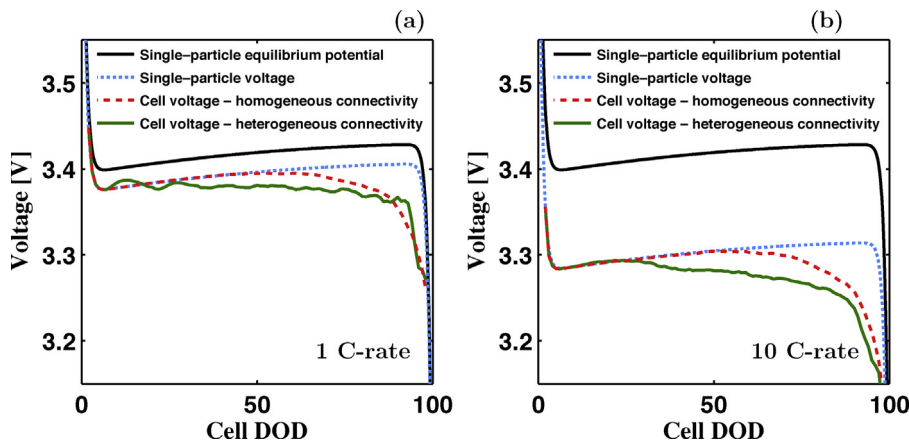


**Fig. 10.** Voltage for discharge (a) at 1 C-rate and (b) at 10 C-rate. The solid and dashed color lines indicate the case of heterogeneous and homogeneous connectivity, respectively. The dotted lines indicate single particle voltage. The heterogeneous connectivity increases the hysteresis between particles: the solid line is generally below the dashed line.

particles in direct contact with the particle. (This dependence and the amount of Li redistribution also depends on the crystal alignment of the contacting particles due to the strong anisotropic diffusivity of LFP [40]; however this is not considered here.) For example, if two particles are in contact, the lithiation of the particle with the larger active surface area to volume ratio will be facilitated as it will extract Li from the other particle. Note that active surface area to volume ratio is correlated to the size of the particles; however, the correlation decreases as the contact between particle increases. The influence of cell architecture on battery performance is apparent here as the spatial arrangement of the particles affects the active surface area to volume ratio and the connectivity of the particles.

The individual DOD of the 200 particles ordered by active surface area to volume ratio is given in Fig. 9 for three different scenarios. Fig. 9(a) shows the DOD of the particles during discharge at 1C. The tendency of particles with larger active surface area to volume ratio to transform early is less apparent due to the heterogeneous connectivity in the dense agglomerate. It is also observable that the transformation of an individual particle occurs in a very short period in comparison with the discharge of the cell. Increasing the discharge rate to 10C does not alter this trend; see Fig. 9(b). The sequential lithiation behavior still prevails at this rate; the only difference with respect to Fig. 9(a) is that each transformation takes a larger fraction of cell discharge time (as indicated by broader transition between blue and red in Fig. 9(b) for each particle). For a direct measurement of the effect of heterogeneous connectivity, we perform an analysis of a dense agglomerate discharged at 1C in which direct redistribution is prohibited (*i.e.*, we artificially homogenize the connectivity). This could correspond to a case in which all particle-particle contacts are not permeable or have a low permeability to Li (*e.g.*, by the presence of carbon coating blocking the contact area). The DOD of the particles resulting from this case is shown in Fig. 9(c). When the particles are homogeneously connected, the order of reaction of particles depends only on their active surface area to volume ratio (similar to the dilute electrode cases).

The cell voltage curves of the dense agglomerate electrode configuration discharged at the two rates considered (1C and 10C) are shown in Fig. 10. Superimposed on each plot are the single-particle equilibrium potential (black solid curve), the voltage curve when the connectivity is homogenized (dashed curve), and the single-particle voltage (dotted curve). The cell voltage for the case with heterogeneous connectivity is slightly lower than that for the case with homogeneous connectivity. This is because heterogeneous connectivity enhances interparticle phase separation, dissipating

more energy by Li redistribution. Unlike in homogeneously connected particles, Li redistribution via direct transport can occur at any C-rate as long as the characteristic timescale of the direct transport is smaller or similar to the characteristic timescale of the discharge process. This process depends on the difference of the chemical potential of the contacting particles and the permeability of the boundary between particles (mathematically expressed in Eq. (7)), and is independent of the driving force for reaction. A schematic of the voltage regimes and corresponding cell behaviors in heterogeneously connected particles are shown in Figs. 7(a) and (b)(ii). Qualitatively, the cell voltage curves for the case with heterogeneous connectivity and the case with homogeneous connectivity (Fig. 10) appear fairly similar. However, the lithiation states of particles can be very different as illustrated in Figs. 9(a) and (c). This fact is alarming because it demonstrates how challenging it is to extract information about the individual particle states from conventional electroanalytical characterization techniques on composite electrodes [4,49].

#### 4.3. Analysis

To quantify the interactions of the particles, we perform several analyses for the dilute agglomerate and the dense agglomerate with homogeneous and heterogeneous connectivity. The dense agglomerate with homogeneous connectivity follows a similar trend as the dilute agglomerate and therefore we do not specifically describe it in these analyses. First, we introduce “effective cycles,” which account for the additional cycling incurred at the individual particle level due to interparticle Li redistribution. Thus, the effective cycles are calculated as the sum of the partial delithiation and redundant re-lithiation of the particles in addition to the full lithiation that occurs during the discharge of the cell. The results are shown in Fig. 11(a). The effective cycles are higher at low currents, and tend to a value of one as current increases. Also, at the given rates, the dilute agglomerate undergoes fewer effective cycles than the dense agglomerate. Second, in Fig. 11(b) we quantify the number of particles reacting simultaneously by counting the number of particles that have an individual DOD between 15% and 85% [50] and then averaging it over the period that the cell has a DOD in the same range. At lower currents, a small fraction of particles react simultaneously while at higher current, the fraction increases. In the dilute agglomerate, a larger fraction of particles react simultaneously than in the dense agglomerate. Note that the fraction of particles reacting simultaneously does not reach 100% at higher currents. This is attributed to the particle size distribution and the resulting difference in active surface area to volume ratio between the particles.

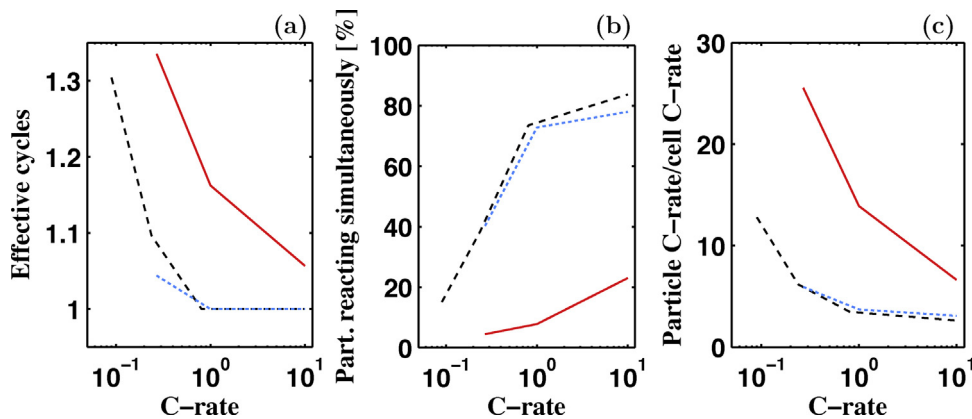


**Fig. 11.** (a) Average effective cycles. (b) Percentage of the particles reacting simultaneously. (c) Average reaction C-rate of the particles compared to the cell C-rate. The dashed lines indicate the dilute agglomerate, the dotted lines are the dense agglomerate with homogeneous connectivity, and the solid lines denote the dense agglomerate with heterogeneous connectivity.

Last, we calculate the ratio between particle C-rate and the cell C-rate which arises due to sequential versus simultaneous particle lithiation; see Fig. 11(c). At lower cell C-rates, active particles lithiate at a rate an order of magnitude greater than the cell C-rate, but this rate difference between cell and particle diminishes at higher cell C-rates. The ratio of particle-to-cell C-rate does not reach a value of one because some particles have larger area-to-volume ratios that lead to earlier completion of lithiation even when the reaction rate (per unit area) is constant.

These three analyses show that (1) homogeneous connectivity and (2) higher rates reduce effective cycles, enhance simultaneous reaction of the particles, and decrease the ratio of the particle C-rate to the cell C-rate of an agglomerate. The results point to the strong influence of the electrode construction (microstructure and connectivity) on electrochemical behavior of the cell. Additionally, contrary to intuition, it is observed that discharging at a higher rate leads to potentially beneficial behavior, which will be discussed further below.

## 5. Discussion

In this work, we have investigated the effect of interparticle Li transport based on the connectivity of the active particles. As previously mentioned, Li redistribution between particles is a source of inefficiency because the free energy reduction associated with Li redistribution does not contribute to the cell voltage. The contribution of connectivity, therefore, extends beyond simply improving bulk transport in the cell, as it determines the amount of Li redistribution. Homogeneous connectivity facilitates *simultaneous* transformation rather than *sequential* transformation of particles, which reduces the local current density of transforming particles (and as a consequence also reduces the overpotential and energy dissipation). High rate performance in LFP electrodes has been observed exclusively when special attention is paid to ensure good electronic and ionic connectivity (notable examples are discussed at length in Ref. 4). This highlights the importance of optimizing multi-particle kinetics in electrode design rather than a single particle alone. For instance, in the dilute electrode (Fig. 5), increasing the rate results in more homogeneous transformation (*i.e.*, each particle DOD approaches the cell DOD). On the other hand, in the dense agglomerate (Figs. 9(a) and (b)), increasing the rate does not have a strong effect, and the amplified local current density within the cell does not reduce significantly when discharged at a higher rate. Since the Li redistribution underlying these observations is intrinsically detrimental to efficient operation of a battery, the effect of heterogeneous connectivity can

potentially explain why high-rate LFP electrodes often require unique electrode architectures that ensure excellent ionic and electronic connectivity between particles [20].

An efficient cell design should minimize Li redistribution. An ideal approach would be a construction where particles are completely isolated from each other but well connected to the electrolyte and current collector. However, since it is unfeasible to construct an electrode where active particles are not connected to each other, the connectivity between particles should be homogenized as much as possible to at least reduce Li redistribution. This can be accomplished by preventing particle agglomeration and therefore enhancing a more uniform spatial distribution. Particle coating may also play a key role in achieving such a result, *e.g.*, by coating of the particles in a way that prevents direct transport. Unfortunately, homogenizing connectivity within a cell typically comes at the cost of reducing the energy density and adding processing steps.

Several experiments support the idea that cell performance can be improved by reducing the interactions between active particles. In the work of Bazzi *et al.* [51], two different cells were compared, one in which particles had uniform coating and remained isolated from each other (Fig. 1(b)), and another in which the coating was non-uniform and particles formed agglomerates with direct particle-particle contacts (Fig. 1(c)). As in our simulations, the former case, which corresponds to the homogeneously connected electrode, exhibited a higher voltage in discharge and capacity than the heterogeneously connected electrode. Also, in the work of Chong *et al.* [19], a significant improvement in the performance of LFP was observed when enough carbon coating was used to fully coat the particles but no significant improvement was found when more carbon coating was used. Moreover, homogeneous connectivity can be achieved by using nontraditional cell architectures, which have been proven to offer an excellent rate performance. Notable approaches include “micro-templating,” which enhances the ionic connectivity by forming a 3D interconnected porous network [52]. Another approach is designing “bicontinuous electrodes,” where uniformly distributed active particles with a tight particle size distribution can be constructed with good electronic and ionic contacts through novel synthesis steps and cell assembly. Such systems have been demonstrated for (dis)charging at very high rate [53]. Improvements to cell design at the microstructural level are discussed in detail in Ref. 54. Since none of these approaches involve modifications of the active materials, the performance improvement clearly stems from the architecture of the cell. While the observed improvements may be caused by the enhancements in electronic and ionic transport, it may also originate from reducing

the interactions between active particles, as indicated by our simulation results.

Our work can help explain the phenomena observed in the scanning transmission x-ray microscopy (STXM) and TEM study of Chueh *et al.* [50]. In their work, a strong concentration inhomogeneity between particles was observed, where the particles were either nearly fully lithiated or delithiated. This observation is consistent with our simulation results, in which there is no nucleation event, and hence these experimental and modeling observations cannot be used to conclude that nucleation is a limiting factor. Another key observation of Chueh's work is that the lithiation state of the particles appears to lack an obvious particle-size dependence. However, a size dependence has been observed in the experimental work of Robert *et al.* [18]. Our model can help reconcile these two different observations. The size dependence in the order of reaction in our simulations is more significant when particles are homogeneously connected and less significant when particles are heterogeneously connected. Thus, we surmise that the connectivity plays a role in the conflicting observations made by Robert *et al.* [18] and Chueh *et al.* [50]. Note, however, that in systems containing large particles (as in these two experiments), bulk diffusion could be the limiting step in the intercalation of the large particles [55], and thus these particles would be less prone to Li exchange and would have a lower dependence on particle connectivities.

Although this work examines the implications for LFP assuming the particles do not undergo intraparticle phase separation, the predictions presented here may still hold qualitatively even if phase separation occurs in some or all the particles. While the particle-size range over which a meta-stable solid-solution path may take place remains a point of debate, there appears to be a consensus that particles with a diameter below ~20 nm would thermodynamically not undergo intraparticle phase separation [56–58], and this value would increase during electrochemical processes because phase separation can be suppressed kinetically [8]. Even if some particles undergo intraparticle phase separation, there will still be a driving force for Li redistribution since monophasic particles (at a Li-rich or Li-poor state) have a lower free energy than phase separated particles within which two phases coexist due to the energy penalty of the interface and the elastic coherency strain. Because of the small size of the particles and the large mobility of Li, the interfaces can be easily moved to the particle surface and then annihilated. Thus, a cell consisting of nanoparticles undergoing intraparticle phase separation may exhibit some of the behaviors observed in this work. More importantly, the findings presented here are also applicable to other nanoparticulate phase-separating materials in which interparticle phase separation is favored.

The simulations performed in this work should be interpreted as a local picture of an electrode, instead of a representation of an entire electrode. The quantitative predictions from this work could differ from the averaged behavior of a real battery for several reasons, such as the small size of the electrode simulated and the specific transport parameters used. In larger cells, the differences in the local electrostatic potential and electrolyte concentration become more significant, leading to a spatial dependence on the order of the reaction of the particles. The group-by-group transformation observed in this work will then occur at different times and different locations in the electrode, depending on different local electrostatic potentials. As a result, the discrete behavior observed here will be smoothed out and the fluctuations of the measured cell voltage would not be observed. Nevertheless, the interactions of the particle occur locally, leading to the increase in the particle C-rates as well as in the effective number of cycles. It is also important to note that the dynamics of charging can differ from those of discharging presented here for several reasons. For example, the asymmetric equilibrium potential considered here, a cathode-activity-dependent exchange current density [26], or

surface energy and curvature effects [48] can all lead to an asymmetric behavior.

## 6. Conclusion

In this study, we explore the consequences of discharging a multi-particle assembly of phase-separating active electrode nanoparticles within an electronic and ionic conducting network, representative of the typical structure of porous Li-ion battery cathodes. Our model includes rich physics and dynamics similar to those experimentally observed in LFP. The simulation results offer a new, alternative explanation of the lithiation process. Unlike in systems where solid solution is the equilibrium state, the state of the electrode (i.e., each particle SOC) cannot be described only by the cell voltage when there exists a thermodynamic driving force for phase separation. In fact, in this model, the multi-particle (de)lithiation path has additional dependence on the cell architecture (or connectivity between particles) and the imposed cell rate. In both homogeneously and heterogeneously connected electrodes, not only do particles transform discretely at low currents upon (dis)charge, but they also undergo Li concentration fluctuations due to Li redistribution between particles. Such discrete transformation leads to three undesired phenomena: amplification of local rates compared to the overall cell rates, increased effective cycles due to redundant cycles, and resulting energy dissipation. At higher rates, however, active particles within the electrode react more simultaneously in a homogeneously connected electrode as the effect of interparticle Li redistribution is reduced. Unfortunately, this improvement at higher rates is contingent on the connectivity of the particles. Heterogeneously connected electrode particles still transform discretely even at these higher rates. These findings highlight the importance of optimizing cell architecture especially in the design of electrodes constructed with nanoparticulate phase-separating materials.

## Acknowledgements

We thank Hao Liu for his valuable comments. This work was supported by the Northeastern Center for Chemical Energy Storage, an Energy Frontier Research Center funded by the U.S. DOE, BES under award number DE-SC0001294. The computational resources were provided by the Extreme Science and Engineering Discovery Environment (XSEDE) (allocation No. TG-DMR110007), which is supported by National Science Foundation grant number OCI-1053575, as well as local computational resources provided by the University of Michigan Advanced Research Computing.

## References

- [1] N. Clark, Boeing Moving Ahead on Making New Planes, The New York Times, <http://www.nytimes.com/2013/06/17/business/global/boeing-moving-ahead-on-new-planes.html?r=0>
- [2] W. Dreyer, J. Jamnik, C. Guhlke, R. Huth, J. Moškon, M. Gaberšček, The thermodynamic origin of hysteresis in insertion batteries, *Nat. Mater.* 9 (5) (2010) 448–453.
- [3] M.S. Whittingham, Lithium Batteries and Cathode Materials, *Chem. Rev.* 104 (10) (2004) 4271–4302.
- [4] R. Malik, A. Abdellahia, G. Ceder, A Critical Review of the Li Insertion Mechanisms in LiFePO<sub>4</sub> Electrodes, *J. Electrochem. Soc.* 160 (5) (2013) A3179–A3197.
- [5] R. Malik, F. Zhou, G. Ceder, Kinetics of non-equilibrium lithium incorporation in LiFePO<sub>4</sub>, *Nat. Mater.* 10 (8) (2011) 587–590.
- [6] P. Bai, D.A. Cogswell, M.Z. Bazant, Suppression of Phase Separation in LiFePO<sub>4</sub> Nanoparticles During Battery Discharge, *Nano Lett.* 11 (11) (2011) 4890–4896.
- [7] T.R. Ferguson, M.Z. Bazant, Nonequilibrium Thermodynamics of Porous Electrodes, *J. Electrochem. Soc.* 159 (12) (2012) A1967–A1985.
- [8] D.A. Cogswell, M.Z. Bazant, Coherency Strain and the Kinetics of Phase Separation in LiFePO<sub>4</sub> Nanoparticles, *ACS Nano* 6 (3) (2012) 2215–2225.
- [9] T. Sasaki, Y. Ukyo, P. Novák, Memory effect in a lithium-ion battery, *Nat. Mater.*, <http://dx.doi.org/10.1038/nmat3623>
- [10] G. Chen, T.J. Richardson, Continuity and performance in composite electrodes, *J. Power Sources* 195 (16) (2010) 5387–5390.

- [11] K.T. Lee, W.H. Kan, L.F. Nazar, Proof of Intercrystallite Ionic Transport in LiMPO<sub>x</sub> Electrodes (M = Fe, Mn), *J. Am. Chem. Soc.* 131 (17) (2009) 6044–6045.
- [12] M. Gaberscek, M. Kzma, J. Jamnik, Electrochemical kinetics of porous, carbon-decorated LiFePO<sub>4</sub> cathodes: separation of wiring effects from solid state diffusion, *Phys. Chem. Chem. Phys.* 9 (15) (2007) 1815.
- [13] J. Liu, M. Kunz, K. Chen, N. Tamura, T.J. Richardson, Visualization of Charge Distribution in a Lithium Battery Electrode, *J. Phys. Chem. Lett.* 1 (14) (2010) 2120–2123.
- [14] H.C. Shin, K.Y. Chung, W.S. Min, D.J. Byun, H. Jang, B.W. Cho, Asymmetry between charge and discharge during high rate cycling in LiFePO<sub>4</sub> - In situ X-ray diffraction study, *Electrochim. Commun.* 10 (4) (2008) 536–540.
- [15] G. Brunetti, D. Robert, P. Bayle-Guillemaud, J.L. Rouvière, E.F. Rauch, J.F. Martin, J.F. Colin, F. Bertin, C. Cayron, Confirmation of the Domino-Cascade Model by LiFePO<sub>4</sub>/FePO<sub>4</sub> Precession Electron Diffraction, *Chem. Mater.* 23 (20) (2011) 4515–4524.
- [16] C. Delmas, M. Maccario, L. Croguennec, F. Le Cras, F. Weill, Lithium deintercalation in LiFePO<sub>4</sub> nanoparticles via a domino-cascade model, *Nat. Mater.* 7 (8) (2008) 665–671.
- [17] M. Ender, J. Joos, T. Carraro, E. Ivers-Tiffée, Quantitative Characterization of LiFePO<sub>4</sub> Cathodes Reconstructed by FIB/SEM Tomography, *J. Electrochim. Soc.* 159 (7) (2012) A972–A980.
- [18] D. Robert, T. Douillard, A. Boulineau, G. Brunetti, P. Nowakowski, D. Venet, P. Bayle-Guillemaud, C. Cayron, Multiscale Phase Mapping of LiFePO<sub>4</sub>-Based Electrodes by Transmission Electron Microscopy and Electron Forward Scattering Diffraction, *ACS Nano* (2013) 1311051123060007, <http://dx.doi.org/10.1021/nm4043964>
- [19] J. Chong, S. Xun, X. Song, P. Ridgway, G. Liu, V.S. Battaglia, Towards the understanding of coatings on rate performance of lifepo<sub>4</sub>, *J. Power Sources* 200 (2012) 67–76.
- [20] B. Kang, G. Ceder, Battery materials for ultrafast charging and discharging, *Nature* 457 (7235) (2009) 190–193.
- [21] S. Chung, J. Bloking, Y. Chiang, Electronically conductive phospho-olivines as lithium storage electrodes, *Nat. Mater.* 1 (2) (2002) 123–128.
- [22] D.-H. Kim, J. Kim, Synthesis of LiFePO<sub>4</sub> Nanoparticles in Polyol Medium and Their Electrochemical Properties, *Electrochim. Solid-State Lett.* 9 (9) (2006) A439.
- [23] C. Delacourt, P. Poizot, J.-M. Tarascon, C. Masquelier, The existence of a temperature-driven solid solution in Li<sub>x</sub>FePO<sub>4</sub> for 0 ≤ x ≤ 1, *Nat. Mater.* 4 (3) (2005) 254–260.
- [24] J.L. Dodd, R. Yazami, B. Fultz, Phase Diagram of Li<sub>x</sub>FePO<sub>4</sub>, *Electrochim. Solid-State Lett.* 9 (3) (2006) A151.
- [25] W. Dreyer, C. Guhlke, R. Huth, The behavior of a many-particle electrode in a lithium-ion battery, *Physica D* 240 (12) (2011) 1008–1019.
- [26] B. Orvananos, T. Ferguson, H.-C. Yu, M. Bazant, K. Thornton, Particle-level modeling of the charge-discharge behavior of nanoparticulate phase-separating li-ion battery electrodes, *J. Electrochim. Soc.* 161 (4) (2014) A535–A546.
- [27] C. Wang, J. Hong, Ionic/Electronic Conducting Characteristics of LiFePO<sub>4</sub> Cathode Materials, *Electrochim. Solid-State Lett.* 10 (3) (2007) A65.
- [28] J. Newman, K.E. Thomas-Alyea, *Electrochemical Systems*, 3rd Edition, Wiley Inter-Science, 2004.
- [29] C.W. Monroe, C. Delacourt, Continuum transport laws for locally non-neutral concentrated electrolytes, *Electrochim. Acta* 114 (2013) 649–657.
- [30] P.M. Biesheuvel, Y. Fu, M.Z. Bazant, Electrochemistry and capacitive charging of porous electrodes in asymmetric multicomponent electrolytes, *Russ. J. Electrochim.* 48 (6) (2012) 580–592.
- [31] S. Dargaville, T.W. Farrell, A comparison of mathematical models for phase-change in high-rate LiFePO<sub>4</sub> cathodes, *Electrochim. Acta* 111 (2013) 474–490.
- [32] R.E. García, Y.-M. Chiang, Spatially Resolved Modeling of Microstructurally Complex Battery Architectures, *J. Electrochim. Soc.* 154 (9) (2007) A856.
- [33] B. Yan, C. Lim, L. Yin, L. Zhu, Three Dimensional Simulation of Galvanostatic Discharge of LiCoO<sub>2</sub> Cathode Based on X-ray Nano-CT Images, *J. Electrochim. Soc.* 159 (10) (2012) A1604–A1614.
- [34] A. Yamada, H. Koizumi, S.-i. Nishimura, N. Sonoyama, R. Kanno, M. Yonemura, T. Nakamura, Y. Kobayashi, Room-temperature miscibility gap in Li<sub>x</sub>FePO<sub>4</sub>, *Nat. Mater.* 5 (5) (2006) 357–360.
- [35] P. Bai, M.Z. Bazant, Charge transfer kinetics at the solid-solid interface in porous electrodes, *Nat. Commun.* 5 (2014) 1–7.
- [36] C.E. Chidsey, Free energy and temperature dependence of electron transfer at the metal-electrolyte interface, *Science* 251 (4996) (1991) 919–922.
- [37] H.-C. Yu, H.-Y. Chen, K. Thornton, Extended smoothed boundary method for solving partial differential equations with general boundary conditions on complex boundaries, *Modell. Simul. Mater. Sci. Eng.* 20 (7) (2012) 075008.
- [38] J. Xie, N. Imanishi, T. Zhang, A. Hirano, Y. Takeda, O. Yamamoto, Li-ion diffusion kinetics in LiFePO<sub>4</sub> thin film prepared by radio frequency magnetron sputtering, *Electrochim. Acta* 54 (20) (2009) 4631–4637.
- [39] Y. Zhu, C. Wang, Galvanostatic Intermittent Titration Technique for Phase-Transformation Electrodes, *J. Phys. Chem. C* 114 (6) (2010) 2830–2841.
- [40] D. Morgan, A. Van der Ven, G. Ceder, Li Conductivity in Li<sub>x</sub>MPO<sub>4</sub> (M = Mn, Fe, Co, Ni) Olivine Materials, *Electrochim. Solid-State Lett.* 7 (2) (2004) A30.
- [41] J. Sugiyama, H. Nozaki, M. Harada, K. Kamazawa, O. Ofer, M. Månnsson, J.H. Brewer, E.J. Ansaldi, K.H. Chow, Y. Ikeda, Y. Miyake, K. Ohishi, I. Watanabe, G. Kobayashi, R. Kanno, Magnetic and diffusive nature of LiFePO<sub>4</sub> investigated by muon spin rotation and relaxation, *Phys. Rev. B* 84 (5) (2011) 054430.
- [42] M. Takeuchi, Y. Kameda, Y. Umebayashi, S. Ogawa, T. Sonoda, S.-i. Ishiguro, M. Fujita, M. Sano, Ion-ion interactions of LiPF<sub>6</sub> and LiBF<sub>4</sub> in propylene carbonate solutions, *J. Mol. Liq.* 148 (2–3) (2009) 99–108.
- [43] M. Tang, H.Y. Huang, N. Meethong, Y.H. Kao, W.C. Carter, Y.M. Chiang, Model for the Particle Size, Overpotential, and Strain Dependence of Phase Transition Pathways in Storage Electrodes: Application to Nanoscale Olivines, *Chem. Mater.* 21 (8) (2009) 1557–1571.
- [44] Y.-R. Zhu, Y. Xie, R.-S. Zhu, J. Shu, L.-J. Jiang, H.-B. Qiao, T.-F. Yi, Kinetic study on LiFePO<sub>4</sub>-positive electrode material of lithium-ion battery, *Ionics* 17 (5) (2011) 437–441.
- [45] V. de Velde E F, Concurrent Scientific Computing, 1st Edition, Springer-Verlag, New York, 1994, pp. p. 202, Ch 8.
- [46] J. Hofhaus, E. VandeVelde, Alternating-direction line-relaxation methods on multicompilers, *SIAM J. Sci. Comput.* 17 (2) (1996) 454–478, doi:[10.1137/S1064827993253872](https://doi.org/10.1137/S1064827993253872).
- [47] T. R. Ferguson, M. Z. Bazant, Phase transformation dynamics in porous electrodes, <http://arxiv.org/abs/1401.7072>
- [48] A. Van der Ven, M. Wagemaker, Effect of surface energies and nano-particle size distribution on open circuit voltage of Li-electrodes, *Electrochim. Commun.* 11 (4) (2009) 881–884.
- [49] M.D. Levi, S. Sigalov, G. Salitra, P. Nayak, D. Aurbach, L. Daikhin, E. Perre, V. Presser, Collective Phase Transition Dynamics in Microarray Composite Li<sub>x</sub>FePO<sub>4</sub> Electrodes Tracked by In Situ Electrochemical Quartz Crystal Admittance, *J. Phys. Chem. C* 117 (30) (2013) 15505–15514.
- [50] W. C. Chueh, F. El Gabaly, J. D. Sugar, N. C. Bartelt, A. H. McDaniel, K. R. Fenton, K. R. Zavadil, T. Tyliszczak, W. Lai, K. F. McCarty, Intercalation Pathway in Many-Particle LiFePO<sub>4</sub> Electrode Revealed by Nanoscale State-of-Charge Mapping, *Nano Lett.*, <http://dx.doi.org/10.1021/nl3031899>
- [51] K. Bazzi, K.S. Dhindsa, A. Dixit, M.B. Sahana, C. Sudakar, M. Nazri, Z. Zhou, P. Vaishnav, V.M. Naik, G.A. Nazri, R. Naik, Nanostructured high specific capacity C-LiFePO<sub>4</sub> cathode material for lithium-ion batteries, *J. Mater. Res.* 27 (02) (2011) 424–430.
- [52] D. P. Singh, F. M. Mulder, A. M. Abdelkader, M. Wagemaker, Facile Micro Tempering of LiFePO<sub>4</sub> Electrodes for High Performance Li-Ion Batteries, *Adv. Energy Mater.*, <http://dx.doi.org/10.1002/aenm.201200704>
- [53] H. Zhang, X. Yu, P.V. Braun, Three-dimensional bicontinuous ultrafast-charge and -discharge bulk battery electrodes, *Nat. Nanotechnol.* 6 (5) (2011) 277–281.
- [54] S.J. Dillon, K. Sun, Microstructural design considerations for Li-ion battery systems, *Curr. Opin. Solid State Mater. Sci.* 16 (4) (2012) 153–162.
- [55] M. Gaberscek, R. Dominko, J. Jamnik, Is small particle size more important than carbon coating? An example study on LiFePO<sub>4</sub> cathodes, *Electrochim. Commun.* 9 (12) (2007) 2778–2783.
- [56] D.A. Cogswell, M. Z. Bazant, Theory of coherent nucleation in phase-separating nanoparticles, *Nano Lett.*, <http://dx.doi.org/10.1021/nl400497t>
- [57] N. Meethong, H.-Y.S. Huang, W.C. Carter, Y.-M. Chiang, Size-Dependent Lithium Miscibility Gap in Nanoscale Li<sub>1-x</sub>FePO<sub>4</sub>, *Electrochim. Solid-State Lett.* 10 (5) (2007) A134.
- [58] M. Wagemaker, D.P. Singh, W.J.H. Borghols, U. Lafont, L. Haverkate, V.K. Petersen, F.M. Mulder, Dynamic Solubility Limits in Nanosized Olivine LiFePO<sub>4</sub>, *J. Am. Chem. Soc.* 133 (26) (2011) 10222–10228.